Górnictwo i Geoinżynieria • Rok 35 • Zeszyt 3/1 • 2011

*Roger Abang**, *Alexander Findeisen**, *Hans Joachim Krautz**

CORROSION BEHAVIOUR OF SELECTED POWER PLANT MATERIALS UNDER OXYFUEL COMBUSTION CONDITIONS

1. Introduction

To ensure effective power generation more plant operations have to be more economical with increased availability, improved efficiency and the lowest possible operating costs. The technologies to be implemented must meet energy policy frameworks, have available resource and capital. For the implementation of efficient and climate-friendly power plant technologies two research and development directions are pursued. These include; increasing efficiency in conventional power plant technologies by raising process parameters and the use of innovative materials for the development of low CO_2 — emitting power plant technologies [1].

Within the framework of ongoing research projects at the BTU Cottbus, the Chair of Power Plant Technology concentrates on process-related investigations, development and evaluation of oxyfuel processes as well as further low CO_2 — emitting power plant technologies. The implementation of oxyfuel processes is achieved by upgrading the plant, including the modification of systems engineering as well as alteration of the associated combustion characteristics. In comparison to conventional combustion conditions, the modified flue gas composition in oxyfuel combustion as a result of the recirculation of the flue gas and the associated high concentrations of the gas species are particularly instrumental for the corrosion process. The prevention and minimisation of possibly damaging processes present a significant challenge for plant operators. To meet this challenge the corrosion mechanisms occurring as a result of the modified process conditions must be analysed and explained.

2. Low CO_2 — emitting power plant technologies

According to the state of the art, a reduction in CO_2 emissions from coal-fired plants could be more than 25% but this cannot be achieved by the use of highly efficient conversion

* Chair of Power Plant Technology, Brandenburgische Technische Universitat Cottbus, Cottbus, Germany

technologies alone. For this purpose, an alternative to reduce emissions is required. A promising option is represented by the research and development of the separation and retention of supplementary CO_2 as a result of low CO_2 — emitting power plant technologies. The carbon dioxide can be separated using various capture processes and subsequently stored or utilised, preventing the CO_2 from escaping into the atmosphere. Depending on the degree of purity of the captured carbon dioxide geological storage in aquifers is possible, it can be used for oil and gas recovery or as a raw material for further processing (e.g. in the food industry). The following will briefly explain the potential capture processes where various pilot and demonstration plants can already be found in various stages of development — planning, construction and operation [2, 3].

3. Basic principles of corrosion

Corrosion is generally the interaction between a material and its environment. Corrosion and the accompanying diffusion of impurities induce measurable changes in the properties of the material and the deterioration of the function of the technical systems [DIN 1999]. These impairments take place for temperatures above 200°C and under the influence of hot gases, steam, dust and ash, and thus, high temperature corrosion occurs. High temperature corrosion can be divided into three individual stages [4]:

1) the release of the corrosion-relevant substances from the fuel in the furnace,
2) the reaction of the compounds formed from the flue gas and flue gas deposits and
3) the reaction of the corrosive medium on the surface of as well as with the metallic materials.

Scale or layer formation as a result of fouling and slagging is a preliminary stage of corrosion and is inseparably bound with fire-side high temperature corrosion [5, 6].

The flue gas-side corrosion in fossil fuel-fired power plants is a known problem that has been present for decades. This seriously impairs power plant operations as a result of material damage in boiler and superheater tubes.

As a result of the high temperature corrosion mechanisms the outer metallic surface is mostly uniformly oxidised and also locally oxidised to form a solid, fluid or gaseous corrosion product. The solid corrosion products are termed oxide layers or scales. The formation of a solid, non-porous and crack-free (protective) oxide layer on the metal can be separated from the gaseous atmosphere. The formation of this protective oxide layer is mostly desired to prevent further corrosion reactions from occurring. Further corrosion reactions are then only possible by the diffusion of reactive components through the oxide layer or by damaging of the protective oxide layer. The formation of cracks and pores in the oxide layer or flaking of the scale due to cyclic thermal stress leads to the acceleration of corrosion processes and thus the rapid failure of the components. In contrast to the protective oxide layer an extremely thick surface layer is formed from slagging and fouling, transporting corrosion-relevant

elements near to the walls. These make corrosion processes possible. The connection between slagging/fouling and corrosion has already been discussed in [7].

The first high temperature corrosion problems were detected in the 1940s in pulverised coal-fired boilers in the USA and are presented in [8]. In Germany, corrosion problems were first noticed in the superheater tubes of the boiler of the Emil Adollf paper mill, as documented by Geiger and Huber [9, 10].

High temperature corrosion in furnaces of steam generators has traditionally been observed in smelting furnaces and is referred to as combustion chamber furnace corrosion [11]. High temperature corrosion is also found in incinerators often used in stoker-fired furnaces. Here the fuel-related high temperature chlorine-based corrosion attacks the unprotected areas of the boiler's heating surface over the furnace grate and the superheater surface of the flue gas path especially when a steam overheating temperature above 350°C is achieved in the latter case [12, 13]. Furthermore, high temperature corrosion is also found in biomass-fired boilers which are mainly used in grate furnaces. The use of residual wood and straw are particularly known to encourage corrosion. Corrosion damage is expected to occur in the flue gas-side of the boiler's heating surface [14, 15].

Unlike in biomass-fired boilers, corrosion in lignite-fired power plants are predominantly caused by the presence of sulphur. In addition to the above mentioned different structural forms of high temperature corrosion, other forms include: salt smelting corrosion, carburisation, internal oxidation, hydrogen attack among others.

Reducing condition corrosion of fuels containing sulphur is a main corrosion mechanism in lignite-fired power plant units. Here, the corrosion takes place in reducing atmospheres under the influence of hydrogen sulphide (H_2S). The H_2S diffuses in the already existing protective oxide layer reacting with iron(III) oxide (Fe_2O_3) to form iron(II) sulphide (FeS) and iron(II,III) oxide (Fe_3O_4). This generates growth stress σ in the oxide layer which leads to the formation of a crack and porous network. The diffusing corrosion-relevant compounds then attack the base materials. Furthermore, an entire part of the protective oxide layer can be removed and thus making the material vulnerable to corrosion attack. The apparent tensional stress is overlaid many times by thermal gradients, leading to frequent layer delamination and thus increasing the removal rate. Subsequently, the formation of a new oxide layer and the beginning of a new corrosion mechanism occur.

4. Corrosion investigations

4.1. Test rig

The investigation of the corrosion behaviour of selected materials was carried out at a 500 kWth pilot plant. Figure 1 shows the process flow diagram of the plant.

The main components of the pilot plant include: an adiabatic 0.5 MWth cycloid combustion chamber (furnace) with tangential firing, a forced draught (FD) fan , a hot gas cyclone with ash cooling screw and cooling circuit, a waste heat boiler (WHB) with air

cooler and circulating pump, a dust filter with an induced draught (ID) fan and chimney. During oxyfuel firing oxygen with a purity of about 99.5% is provided from a tank (no air separation unit). Part of the flue gas that is not recycled is drained into a flue gas condenser with an integrated cooling circuit.

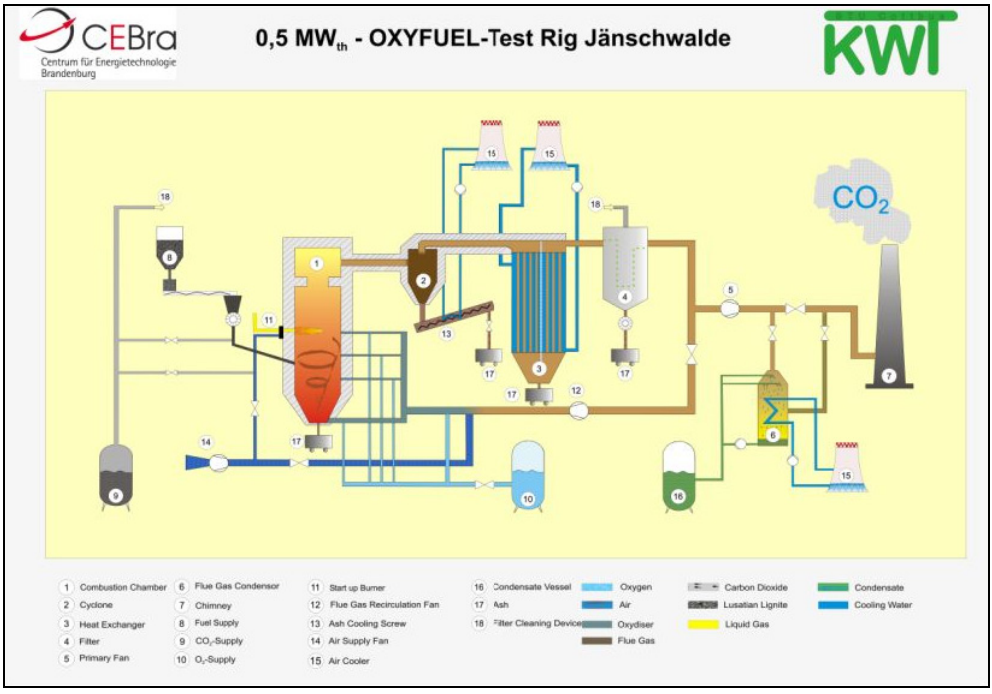

Fig. 1. Process scheme of the 500 kWth pilot plant at Jänschwalde

Dried Lusatian lignite with a particle size distribution of 0 to 6.3 mm and water content of 19wt% is used as the primary fuel. The fuel is fed into the combustion chamber tangentially via a fuel-feeding system that consists of a double through screw conveyor, a double paddle mixer, two tube screw conveyors, volumetric dosing, a rotary feeder and downpipes. The fuel-feeding system is also designed for use with alternative fuels (e.g. sludge or wood chips). The alternative fuel is then mixed in the double paddle mixer with the dried lignite and then fed into the combustion chamber. The addition of the desulphurisation additive (for dry desulphurisation) is possible and this can be done in the double through screw conveyors so that the additive and the fuel reach the furnace at the same time.

The oxidising agent (depending on operating mode of operation could be: fresh air, fresh air with recycled flue gas or pure oxygen with recycled flue gas — oxyfuel) is brought into the combustion chamber by the FD fan, the flue gas recirculation fan and then distributed

into the various air levels: rotary air, primary air and three secondary air levels. During oxyfuel operation oxygen could be fed into the main oxidising stream (mixed with recycled flue gas) or sent directly into the different air levels to regulate the amount of O_2 entering each air level — for process optimisation.

After combustion the hot flue gas leaves the furnace at a maximum temperature of about 950°C and is first cleaned of coarse ash particles in the hot gas cyclone before being sent to the WHB for cooling. In the WHB, the flue gas is cooled-down to filter-compatible temperature of 130÷250°C. For further flue gas cleaning, a conventional fabric filter and the ID fan are used, such that a cooled and dust-free flue gas can be released via the chimney into the surroundings. The flue gas removal for flue gas recirculation takes place between the fabric filter and the ID fan. The flue gas condenser is located in the bypass between the ID fan and the chimney. During oxyfuel operation the water which accumulates in the process is condensed-out and removed in the flue gas condenser.

With the combustion of lignite, residual ash is deposited in various locations in the system. Coarse and/or unburned, inert particles which are deposited in the lower part of the furnace are easily removed. A large proportion of the ash in the flue gas from the furnace is removed and separated from the flue gas stream in the hot gas cyclone. The resulting hot ash is first cooled-down below the cyclone in an integrated water-cooled ash cooling screw from 940 to 40°C. To prevent ash deposits in the flue gas tubes of the WHB an acoustic noise horn is integrated. The ash that is deposited in the WHB is collected in an ash container. After the WHB the remaining ash particles are separated to the greatest possible extent in dust filter and are sent over a rotary feeder into a bulk container.

The WHB is used as a dual flue gas tube boiler. The flue gas is led through the flue gas tube and cooled against the wall within which circulates cooling water. The cooling water is then heated-up at 6 bar to a max. temperature of 110°C. The hot cooling water is subsequently cooled-down in an air cooler against the surroundings to approx. 80°C.

The flue gas condenser for the separation of water contained in the flue gas (up to 30wt%) consists of a quencher and a cooler. The cooled flue gas exits the condenser over a droplet separator.

To minimise air-inleakage (false air) in the plant, CO_2 supplied from a tank is used as purge-gas. The purge gas is usually used in the cooling down of the liquefied-gas burner, the pulse jet cleaning system of the tube filters, the compressed air supply of the acoustic noise horn and the cleaning of the fuel feed.

The pilot plant is equipped with several measuring devices for complete mass and energy balance evaluations. These include temperature and pressure measurements in the furnace and the oxidant gases, the flue gas and cooling water pipes as well as the flue gas stream after the furnace and before the WHB. All measurements are recorded and saved in a process control system and can subsequently be evaluated. The overall process is controlled and supervised by a computer-aided process control system.

4.2. Laboratory test rig

The laboratory test rig consists of a gas mixing station, a tube furnace with an air-cooled lance and an evaluation unit as shown in Figure 2 below.

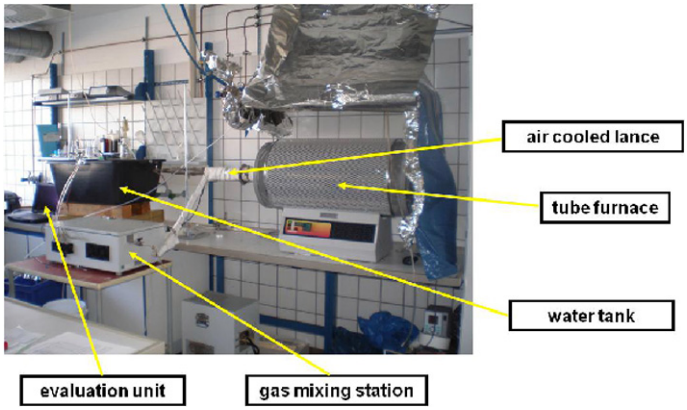

Fig. 2. Basic layout of the laboratory setup

The tube furnace from Carbolite (type: STF 15/450) is a horizontal furnace with a maximum operating temperature of 1.500°C and a heated length of 450mm. The Al_2O_3 — working tube has an inner diameter of 75 mm and is heated by parallel silicon carbide heating elements that are arranged on the outside.

The gas mixing station is a PC-controlled gas mixing system from QCAL Messtechnik GmbH, which enables different individual gases to be mixed using a mass flow controller (MFC) and enabling the integrated boiler to add steam to the gas mixture via the MFC.

TABLE 1
Gas species and the MFC dosing range

Gas Species	MFC Dosing Range
Nitrogen N_2	0.2…19 l/min or 0.6…64 cm³/min
Oxygen O_2	4.6…481 cm³/min
Carbon dioxide CO_2	0.1…10.7 l/min
Sulphur dioxide SO_2	0.75…37.4 cm³/min
Hydrogen sulphide H_2S	0.54…26.7 cm³/min
Water H_2O	0.6…600 g/h

The mixing station was supplied with gas from a closed circular pipeline adjacent to the laboratory i.e. directly from the connected gas cylinders. The following gas qualities were used — Table 2).

TABLE 2
Gas qualities used

Gas Species	Purity, vol%
Nitrogen N_2, 5.0	$\geq$ 99.999 (incl. noble gases)
Oxygen O_2, 5.0	$\geq$ 99.999
Carbon dioxide CO_2, 3.0	$\geq$ 99.9
Sulphur dioxide SO_2, 3.8	$\geq$ 99.98
Hydrogen sulphide H_2S, 2.5	$\geq$ 99.5

It can be seen that some gases (N_2 and O_2) were introduced via the gas species CO_2 and H_2S. However, these impurities did not cause any significant changes and as such the fugacities were not substantially altered.

Purified drinking water was used and a two-stage processing occurred upstream. The drinking water was then desalinated using a mixed bed cartridge and then further processed using a Reinstharz cartridge. Accordingly, a water quality of 0.055 µS/cm at 25°C was achieved.

After exiting the gas mixing station the gas mixture flows over an externally heated stainless steel tube directly into the working tube and was ready for corrosion reactions to occur. Inside the working tube was a gas-permeable Al_2O_3 — plate in the form of a half-shell supporting the ash bed. The probes were placed such that approximately a third of the circumference of the probe was in the ash bed and the remainder came directly into contact with the gas mixture. The ash used was ash from obtained from the hot gas cyclone from the 110 hours experiment at the test facility at Jänschwalde. The sample area positioned in the ash bed was referred to as the "south side", while the "north side" was the area exposed only to the gaseous atmosphere and the inherent residual ash. Thus, the probe could be placed both with and without contact to ash.

The air-cooled lance that supported the probe was introduced into the working tube together with the auxiliary structure and the internal structure as shown in Figure 3. To maintain the temperature, the ends of the working tubes were padded with insulating wool and sealed in a gas-tight manner. Therefore, apart from direct gas supply to the probes, indirect gas supply through the reactive ash bed was also possible. Furthermore, the gaseous waste from the working tube could be condensed and emitted via an outlet.

TABLE 3
Chemical composition of the selected materials, wt%

Steel	C	Ni	Mn	O	Mo	Fe	Cr	Cu	Si	W	Co
16Mo3	0.31	0.04	0.73	0.04	0.27	98.43	0.09	–	0.14	–	–
13CrMo4-5	0.74	0.02	0.58	0.02	0.27	96.93	0.95	0.07	0.41	–	–
7CrVTiB10-10	0.17	0.11	0.71	0.002	0.97	95.46	2.35	–	0.23	–	–
10CrMo9-10	0.25	0.07	0.42	0.01	0.85	96.08	1.98	0.13	0.22	–	–
VM12 SHC	0.23	0.28	0.36	–	0.25	83.01	12.01	–	0.30	1.43	1.47

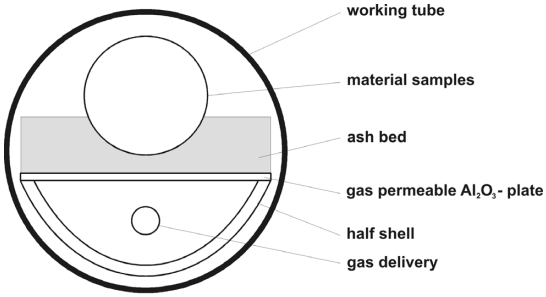

Fig. 3. Schematic cross-section of the position of the probe

4.3. Material characterisation

For the corrosion investigation the following boiler materials; 16Mo3, 13CrMo4-5, 7CrVTiB10-10 and superheater materials; 10CrMo9-10, VM12 SHC were selected. The analysis of the corroded probes was conducted at the Federal Institute for Materials Research and Testing, Department V, Division V.1 — Composition and Microstructure of Engineering Materials. Tubing test probes with dimensions of 51 × 4 mm × 30 mm (outer diameter × wall thickness × length) as well as a reference probe were prepared from the materials. In Table 3, the selected materials and their chemical compositions are shown. Analyses were carried out using an electron beam spectroscopy (microprobe type JEOL-microprobe JXA-8900 RL). The uncertainty of the microprobe was 0.01–0.02wt%. Analysis of composition was carried out at 12 different measuring points on each probe and the acquired values were subsequently averaged.

5. Results

5.1. Results after 110 hours exposure time

Within the framework of conducting the analytical research, the ash from the hot gas cyclone was investigated, assessing the chemical and crystalline composition. After an initial assessment, the probes were analysed by a light and scanning electron microscope (SEM).

With regard to chemical composition, the analysis of the ash displayed no significant differences, which is why additional x-ray diffraction investigations were conducted. In doing so all crystalline phases, including elements from the chemical analysis were analysed. The X-rays showed that in both ash probes (oxyfuel and air conditions) the same phases exist. However, the single phases showed different concentrations. As illustrated below, it can be seen which ash (air or oxyfuel) had higher phase components:

— Calcium sulphate $CaSO_4$ air
— Quartz SiO_2 oxyfuel
— Magnetite Fe_3O_4 air

— Hematite Fe_2O_3 air
— Maghemite Fe_2O_3 oxyfuel
— Periclase MgO same
— Siderite $FeCO_3$ air.

The refined maghemite, a defect structure of magnetite, forms either under reducing conditions (with CO present) or when steam is present. This development is similar to the placement experiments under artificial atmospheres in [16]. The low amount of siderite in the oxyfuel ash suggests that the formation of a closed and protective carbonate layer is not possible.

The identified differences in the phase components suggest that the ash has different concentrations in the corrosion-relevant phases for reactions. Therefore, different corrosion behaviour under the different operating conditions was expected. The melting temperature of the oxyfuel ash is approx.

50 K higher than in air combustion conditions, and therefore, there is a higher tendency of slagging in conventional air firing than in oxyfuel.

In [17], comparative modelling is evaluated with the software FactStage with respect to ash composition under different combustion conditions. The analysis showed that for a combustion temperature of 700°C similar ash concentrations are expected whereas at a temperature of 500°C an increase concentration in sulphates was evident. Furthermore, the influence of the excess oxygen and sulphur content were modelled. With regard to excess oxygen it was shown that for sub-stoichiometric and over-stoichiometric combustion conditions for the above mentioned temperatures the same ash composition is obtained. Solely under conventional (air) combustion conditions and with $\lambda < 0.75$ led to an increase in unburnt ash. Furthermore, the modeling also showed that the ash composition is primarily dependent on the sulphur content in the flue gas. Therefore, with an increase in the sulphur content a higher proportion of sulphur was recorded in the ash.

As already mentioned, the light microscope was used to analyse layer thickness but no exact layer thickness could however be determined from the light microscopic analysis due to the partially damaged and porous (the oxide layer was partially destroyed were characterised by higher porosity) oxide layers. The major reason for this was the flaking of the ash and oxide layer both during romoval of the probes from the furnace and also in the transport and preparation process. Thus sufficient, accurate measurements were not possible and the interpretation of present results (on the progression of corrosion) was difficult. Only the measurement of the remaining wall thickness which to date was not carried out could provide some information about the progression of corrosion.

With regard to corrosion behaviour the SEM-micrographs including an EDX line-scan of the detailed probe showed hardly any difference between high and low placed probes. This is often the case when initial corrosion which requires 200 to 250 hours to obtain a significant corrosion (here only 110 hours) occurs without a layer in the reaction equilibrium with the surrounding. Additionally, the low material temperature of 490°C did not allow the

rapid formation of chromium scales even with a high chromium ratio in the alloy. However, it was apparent that with increasing chrome content in the alloy a considerable concentration of chrome could be seen on the inner oxide layer. The chrome reacts with iron and oxygen to form iron spinels as well as chromium oxide which are thick and act as protective layers. However, an increase in the chromium content and greater placement timeframe showed a decline in corrosion activity.

5.2. Results after 1100 hours exposure time

As already mentioned, the probes were analysed sing light and scanning electron microscopes (SEM) at the Federal Institute for Minerals Research and Testing in Berlin. In preparation for the analysis the probes were embedded in epoxy resin and cross-sections were cut. The light microscopy analysis to record the structure of the surface layer was performed using a Reichert MeF3A reflected-light microscope. The SEM images (device type LeoVP1530) were used to analyse the composition of the phases from the oxide layer to the base material (so-called line-scans) and point analysis were also conducted. Furthermore, the light microscopic images were etched with a V2A-etchant so that possible carburisation processes could be clearly depicted.

Selected results from the above mentioned methods shall be presented and discussed in the following sub-sections. The images of the probes will precede the respective explanations and the numbers on the images refer to particular points in the SEM.

5.2.1. Material 16Mo3

The light microscopic images showed porous surface layers as well as loose, overlying and partly-flaked layers of ash under both operating conditions. The main components of the porous surface layer were hematite (Fe_2O_3) and magnetite (Fe_3O_4). Iron (II) sulphide (FeS) could not be confirmed. A comparison of the thickness of the layers showed similar layer thickness of the probes on the north side under both air and oxyfuel. However, under oxyfuel conditions the thickness of the layer on the south side was considerably greater than that on the north side. This was due to the existing ash bed and the reactive components within it as can be seen in the SEM image of the material 16Mo3 (Fig. 5).

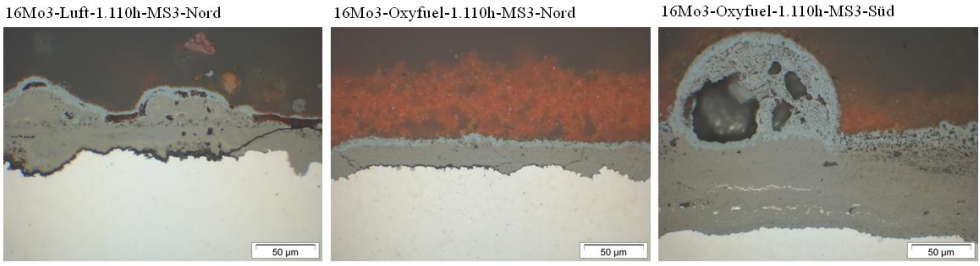

Fig. 4. Light microscope image of the material 16Mo3

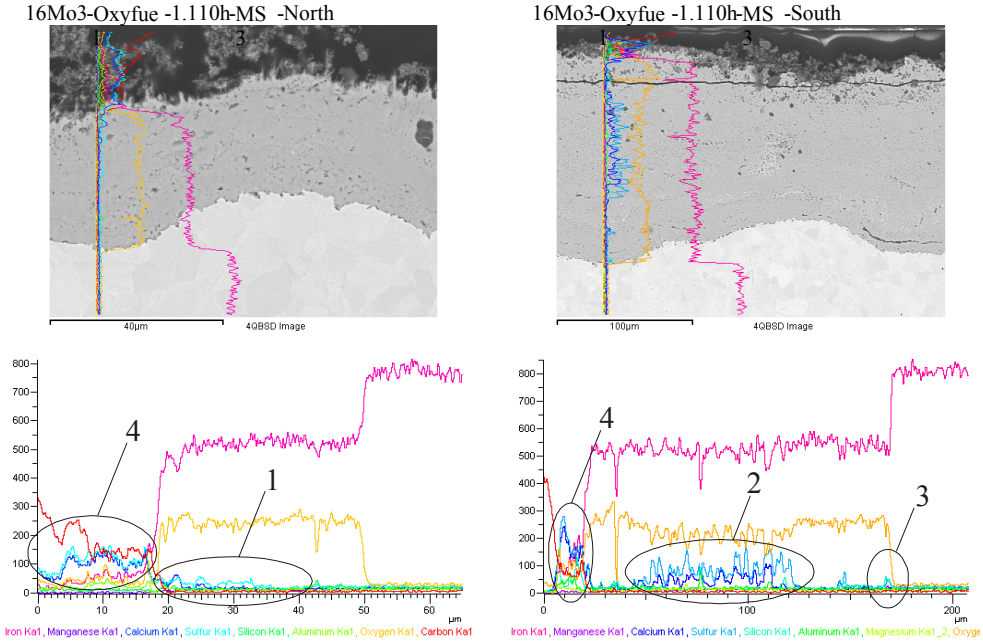

Fig. 5. Scanning electron microscope image of the material 16Mo3

Furthermore, the SEM images indicated that under oxyfuel conditions sulphur formed on the surface layers. Therefore, the embedding of the probe in the ash bed seemed to have increased the depth of the inward diffusion of sulphur (see 1 and 2 in Fig. 5). Moreover, sulphur was also present in the partially existing layers of ash (see 3 in Fig. 5). In all cases sulphur peaks were accompanied by calcium peaks. This suggested that sulphur was present as calcium sulphate ($CaSO_4$). However, the bonding of sulphur to calcium under oxyfuel conditions was less pronounced which therefore means that other metal-sulphur compounds may have been formed (compare 2 and 4, Fig. 5).

5.2.2. Material 13CrMo4-5

Under both operating conditions the surface layer was characterised by loosely attached formations of ash that were partially flaked. The outer layer of corrosion was covered with many tiny pores. Apart from the tiny pores under oxyfuel conditions, the inner layer of corrosion also had a few large pores. Furthermore, the images indicated that under oxyfuel conditions on both the north and south sides, the inner oxide layer extended along the grain borders.

The main components of the defining surface layers were hematite (Fe_2O_3) and magnetite (Fe_3O_4) as well as the first Fe-Cr spinels, resulting from the chromium present in the base material. This could be accounted for by iron (II) sulphide (FeS) under oxyfuel conditions (see 1 in Fig. 7).

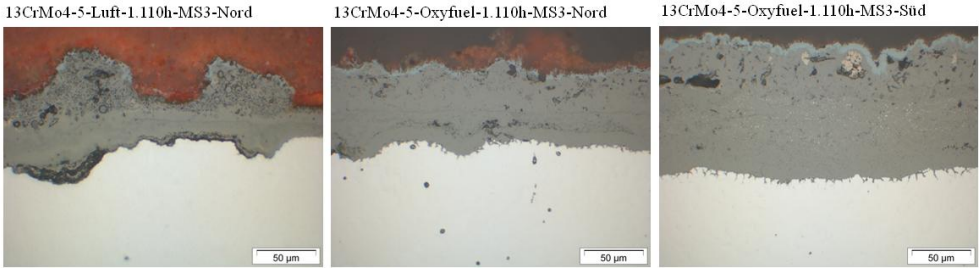

Fig. 6. Light microscope image of the material 13CrMo4-5

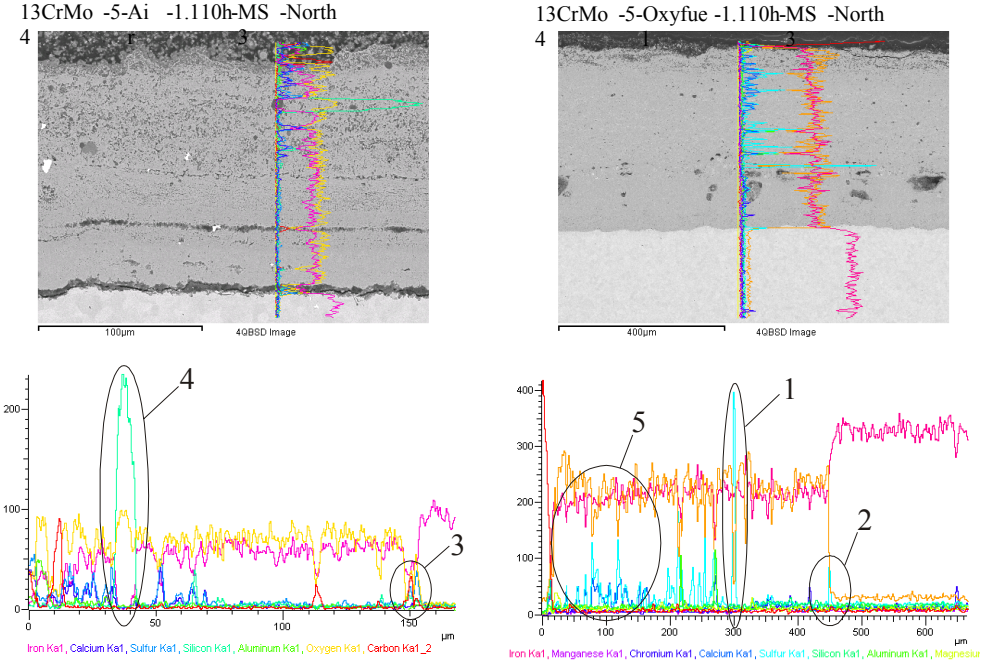

Fig. 7. Scanning electron microscope image of the material 13CrMo4-5

This can be seen especially from the sulphur peaks, the steady iron components and the decreasing oxygen components. The comparison in layer thickness showed similar results in both the north and south side under air and oxyfuel conditions. However, the thickness of the layers in the south side under oxyfuel conditions was considerably greater than on the north side. Again this was due to the existing ash bed and the reactive components within it.

The SEM images showed that sulphur was present under both operating conditions for the entire cross-section of the line-scan. The existence of sulphur near the interface of the base material / oxide layer indicated that the Fe-Cr spinels were permeable and therefore

not protective (see 2 and 3, Fig. 7). The existing sulphur found at the interface comprised of ash particles with a high amount of silicon (see 4, Fig. 7) which indicates that the sulphur was sulphate-bound. The parallel presence of sulphur, chromium and iron as well as the decrease in oxygen (O_2) under oxyfuel conditions indicated that iron-chromium-sulphate compounds (CrS_2, FeS) and presumably also chromium sulphides ($Cr_2(SO_4)_3$) were formed (see 5, Fig. 7).

5.2.3. Material 10CrMo9-10

From the light microscopic images in Figure 8, it could be seen that only loosely attached formations of ash with flakes were present on the probes. Under air conditions the underlying corrosion layer was characterised by a few large pores and numerous tiny pores. However, under oxyfuel conditions large pores were evident in the outer corrosion layers while the inner corrosion layers exhibited hardly any pores. The image of the north side under oxyfuel conditions showed a concentration of the large pores on the interface between the outer and inner corrosion zone. The main components of the differentiable surface layers were hematite (Fe_2O_3), magnetite (Fe_3O_4) as well as a few Fe-Cr spinels. The clearly pronounced, elongated growth of the hematite layer on the north side under oxyfuel conditions was primarily a result of the perfectly functioning gas diffusion within the oxide layer. In addition, it is assumed that under both conditions there is specific formation of iron sulphide within the surface layer (see 1 and 2).

Inspection of layer thickness indicated a significantly lower thickness for probes under air conditions. Furthermore, the oxide layer on the south side under oxyfuel conditions was significantly greater than on the north side. Layer thickness was similar for probes located on the north side under oxyfuel conditions. By contrast layer thickness under oxyfuel conditions on the south side was significantly greater than on the north side. This was due to the existing ash bed and the reactive components contained within it.

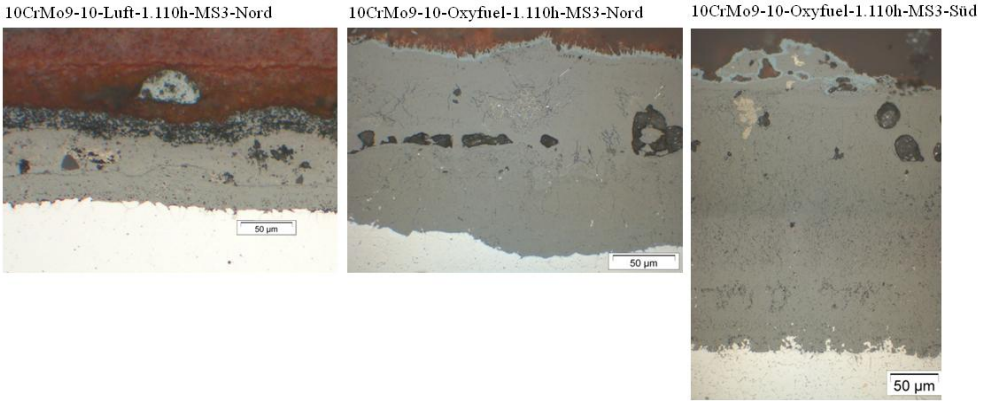

Fig. 8. Light microscope image of the material 10CrMo9-10

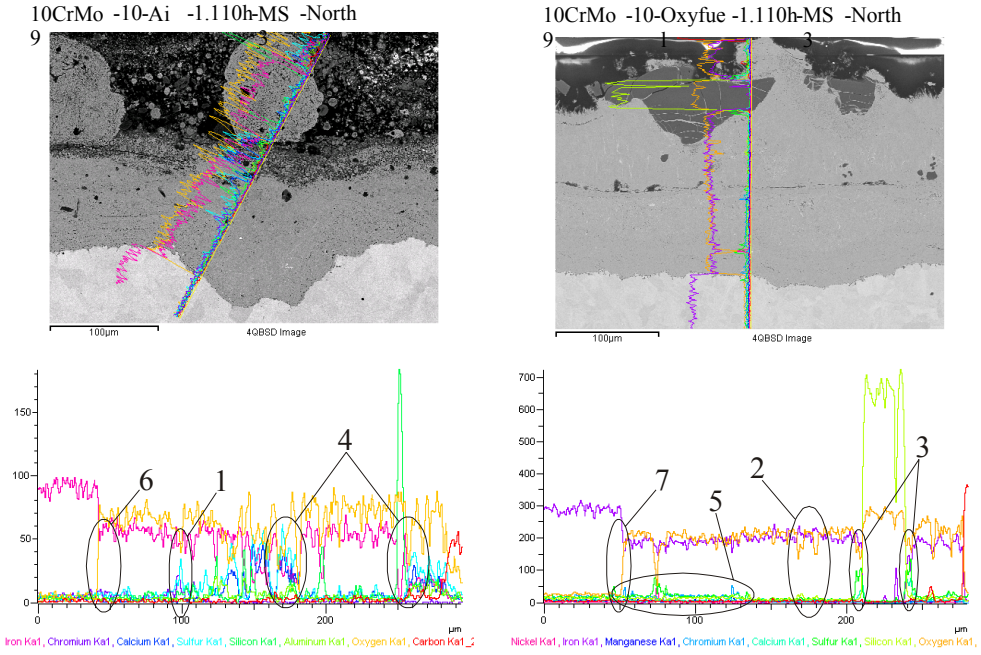

Fig. 9. Scanning electron microscope image of the material 10CrMo9-10

Inward diffusion of sulphur into the ash and oxide layers occurred under both operating conditions. The formation of sulphuric acid in connection with calcium in the border areas around ash particles could be seen (see 3 and 4, Fig. 9). In the line-scan of the north side under oxyfuel conditions a distinct chromium-rich inner corrosion zone was identifiable (see 5, Fig. 9). The parallel presence of sulphur, chromium and iron as well as the decrease in oxygen under oxyfuel conditions indicated the formation of iron-chromium-sulphate compounds (CrS_2, FeS) and presumably also chromium sulphides ($Cr_2(SO_4)_3$) (see 5, Fig. 9). However, the formation of a thick and protective layer of Fe-Cr spinels was not possible because sulphur was present up to the border of the base material / oxide layer. The sulphur present could be sulphate- or sulphide-bound (see 6 and 7, Fig. 9).

5.2.4. Material 7CrVTiB10-10

The ash formations present on the probes were only loosely attached and were characterised by a considerable amount of flakes. Furthermore, the oxide layer featured a cracked structure covered with many tiny pores. This was however not a characteristic feature for all probes. However the 7CrVTiB10-10 probes did exhibit a characteristic oxide layer that was comparable to the other probes that were observed. The main components of the differentiable surface layer featured hematite (Fe_2O_3) and magnetite (Fe_3O_4) as well as Fe-Cr spinels.

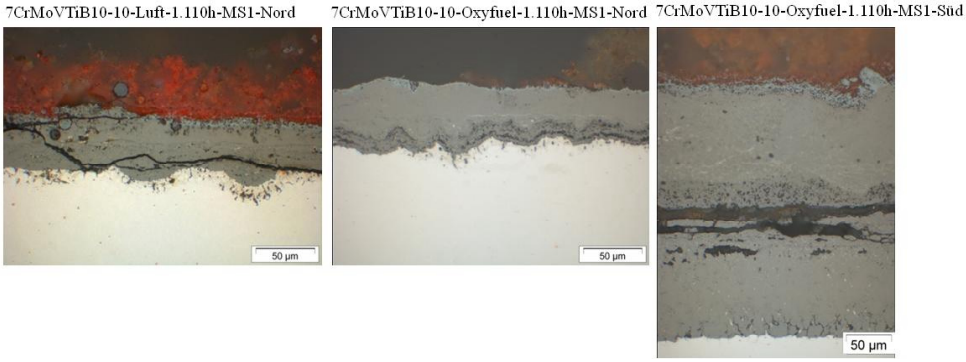

Fig. 10. Light microscope image of the material 7CrVTiB10-10

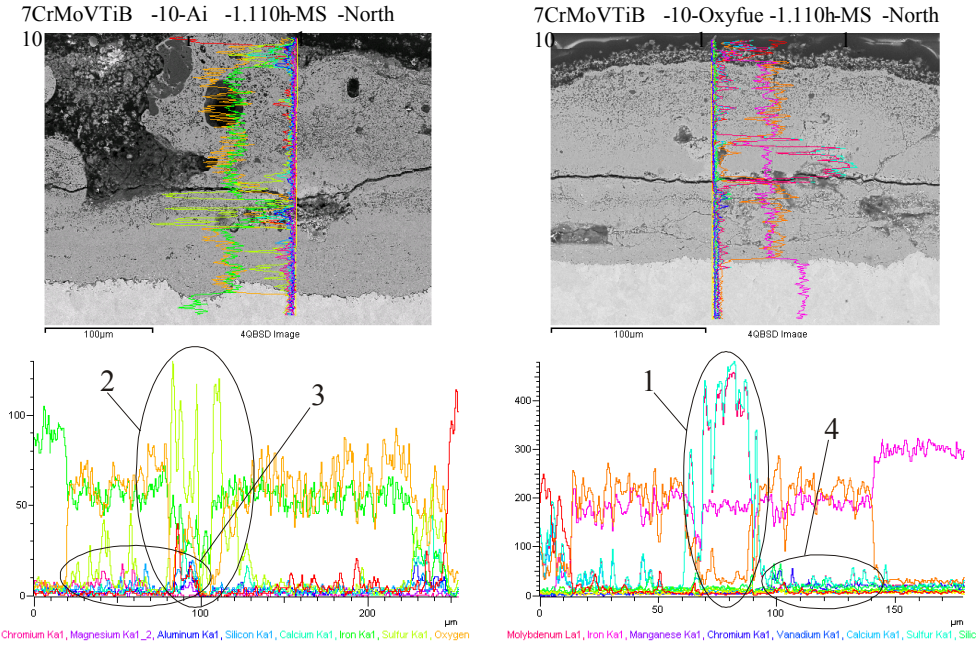

Fig. 11. Scanning electron microscope image of the material 7CrVTiB10-10

The thickness of the oxide layer on the north side of the probes under air conditions in comparison to oxyfuel conditions was smaller. Moreover, under oxyfuel conditions layer thickness on the north side was markedly smaller than on the south side.

The formation of a crack extending along the periphery resulted in a considerable concentration of sulphur on both sides of the crack. Therefore, under oxyfuel conditions the

formation of iron sulphide was unequivocal. The formation of an iron sulphide phase was due to the increase in sulphur bonded with the simultaneous decrease in oxygen components and the unaltered number of iron components in this zone. In contrast to this, the sulphur components were sulphate- and sulphide-bound under air conditions. Iron and sulphur were both present but there was also a significant decrease in the concentration of oxygen and thus, it was assumed that iron sulphide could also be present. Directly beside this iron, sulphur and calcium as well as some oxygen could be accounted for and so the formation of calcium sulphate and iron sulphide occurred (see 2, Fig. 11).

The underlying crack in the oxide layer was found under both operating conditions around the inner corrosion layer, which was evident from the considerable deposits of chromium. Sulphur was present on the inner corrosion layer up to the interface between the base material and oxide layer but which did not originate from a thick and non-protective layer of Fe-Cr spinels (see 3 and 4, Fig. 11).

The parallel presence of sulphate, chromium and iron and the reduction in oxygen and the formation of iron-chromium-sulphate compounds (CrS_2, FeS) and presumably also chromium sulphides ($Cr_2(SO_4)_3$) were found in the material under air conditions (see 3, Fig. 11). This was contrary to the results from the materials 13CrMo4-5 and 10CrMo9-10, where the described phases were only present under oxyfuel conditions.

5.2.5. Material VM12SHC

The ash present on the probes was loosely attached and partly flaked. Under air conditions an outer corrosion layer covered with pores formed on the probes. The inner layer of corrosion was characterised by a border of non-corrodible residual materials whereas the base material was locally attacked. The oxide layer originating from oxyfuel conditions featured a clear distinction between inner and outer corrosion layers. Apart from the existing pores there was a strong network of cracks throughout the outer corrosion layer. Under oxyfuel conditions these reached from the south side to the inner corrosion layer. Under oxyfuel conditions, non-corrodible residual materials were present in the inner corrosion layer in the form of a border in both the north and south side. In contrast to air conditions, the base material in oxyfuel exhibited a localised and more pronounced corrosion attack. The formation of a border occurred as a result of corrosion along the grain border due to the formation of chromium-rich oxides. The characteristic shape decreased when changing from air to oxyfuel atmospheres. It also decreased from north to south under oxyfuel conditions. This observation can be explained by the increased oxidation of the chromium-rich insular residual base materials in the surface layer under oxyfuel conditions.

The main components of the surface layer included hematite (Fe_2O_3) and magnetite (Fe_3O_4) as well as an increasing number of Fe-Cr spinels. No evidence could be found for the formation of a sulphide phase. The thickness of the oxide layer on the probes under air conditions was comparable to those on the north side under oxyfuel conditions. The same figure shows the comparison between the north and south sides under oxyfuel conditions.

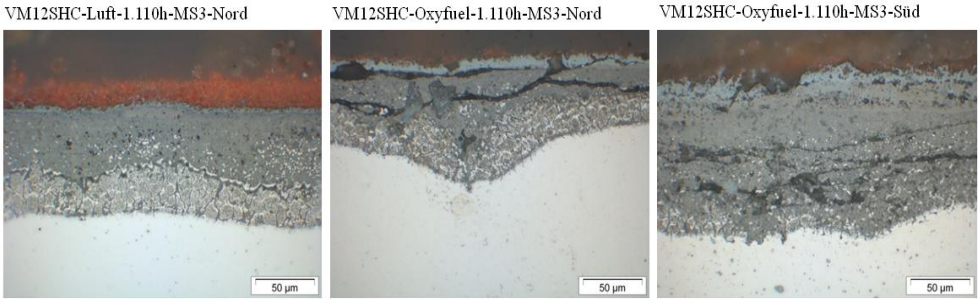

Fig. 12. Light microscope image of the material VM12 SHC

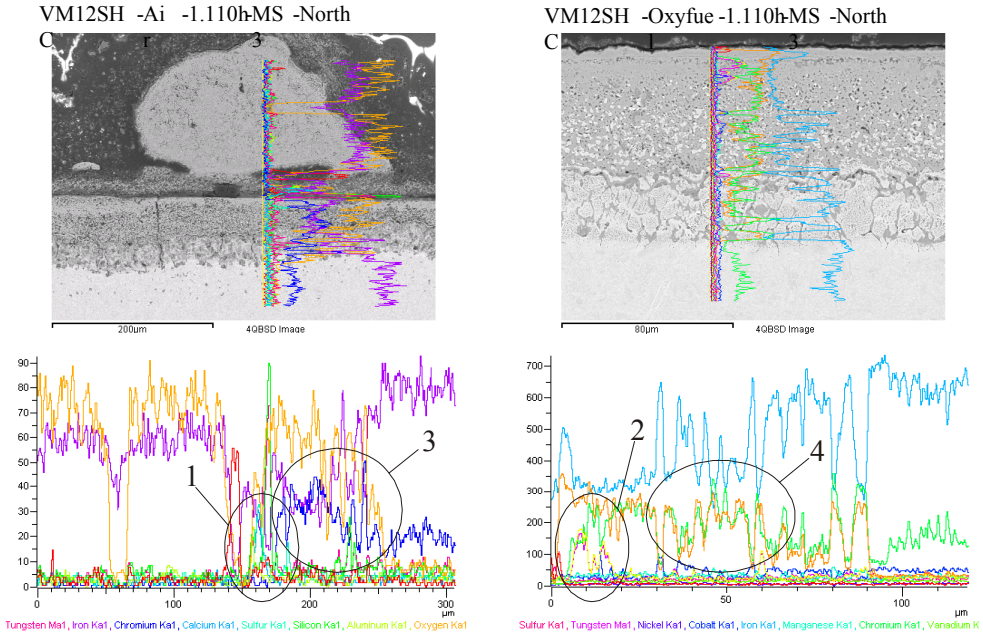

Fig. 13. Scanning electron microscope image of the material VM12 SHC

The VM12 SHC probe displayed similar sulphur formation characteristics under both operating conditions. These were sulphate-bound within the oxide layer (see 1 and 2, Fig. 13). Therefore under air conditions further phases were present and so area 1 (Fig. 13) displayed a loose, porous layer. No sulphur peaks were found at the interface between the base material and the oxide layer and this was due to the increased formation of Fe-Cr spinels thus the associated passive effect of sulphur diffusion. Under oxyfuel conditions a significant formation of Fe-Cr spinels was apparent (see 3 and 4, Fig. 13).

Under air conditions the SEM images featured ash particles that had accumulated above the oxidised surface layer. Between the particle and the surface layer no reaction-dependent interactions were evident. It was therefore assumed that a non-reactive surface layer had formed.

6. Summary

In the framework of this project the exposure of the pre-corroded probes 16Mo3, 13CrMo4-5, 10CrMo9-10, 7CrMoVTiB10-10 and VM12SHC for a timeframe of over 1,000 hours was performed at the Chair of Power Plant Technology's laboratory test rig at the BTU Cottbus. Initial corrosion of the probes was carried out over a period of 110 hours in a test facility. In both experiments, the probes were investigated under air and oxyfuel combustion conditions. Subsequently, the probes were analysed using light and scanning electron microscopes at the Federal Institute for Materials Research and Testing in Berlin. With the help of light microscopic images characterisation of the oxide layers that formed as well as analysis of wall and layer thickness was possible. By means of SEM images phase composition using point analysis as well as line-scans could be examined.

The investigations indicated that oxyfuel conditions enhanced the corrosion of the material and therefore this phenomenon requires particular attention. However, the relatively short timeframe of 1.110 hours demonstrated only the tendencies for corrosion. To gain a better understanding and obtain concrete material-specific conclusions long-term trials of over 4,000 hours of exposure time must be conducted. Furthermore, the operating parameters could be also adjusted e.g. adjusting temperatures for the operating conditions of the material and observing the change in the individual alloys such as molybdenum in 16Mo3.

REFERENCES

[1] BMWI 2007 — Bundesministerium für Wirtschaft und Technologie. Leuchtturm COORETEC — Der Weg zum zukunftsfähigen Kraftwerk mit fossilen Brennstoffen, Forschungsbericht Nr. 566, Berlin 2007

[2] BMWI 2003 — Bundesministerium für Wirtschaft und Technologie: "Forschungs und Entwicklungskonzept für emissionsarme fossil befeuerte Kraftwerke" Forschungsbericht Nr. 527, Berlin 2003

[3] ZEF 2006 — Zentrum für Energieforschung: Endbericht „Neubau fossil gefeuerter Kraftwerke — Versorgungssicherheit, Wirtschaftlichkeit, CO_2-Reduzierung" Stuttgart 2006

[4] *Born M.*: Dampferzeugerkorrosion ISBN 3-934409-27-X Verlag SAXONIA Standortentwicklungs und Verwaltungsgesellschaft mbH Freiberg 2005

[5] DIN 1999 — Normenausschuss Materialprüfung (NMP) im Deutschen Institut für Normung e.V.: DIN EN ISO 8044 Korrosion von Metallen und Legierungen — Grundbegriffe und Definition Beuth Verlag Berlin 1999

[6] IKD 1996 — Institut für Korrosionsschutz Dresden: Vorlesung über Korrosion und Korrosionsschutz von Werkstoffen Teil I; ISBN 3-930526-05-0; TAW-Verlag Wuppertal 1996

[7] *Gumz W.*: Kurzes Handbuch der Brennstoff- und Feuerungstechnik 3. Auflage Springer-Verlag Berlin /Göttingen/ Heidelberg 1962

[8] *Corey R.C., Reid W.T., Cross B.J.*: External Corrosion of Furnace-Wall Tubes — History and Occurence Transactions of the ASME 67 1945 p. 279–302

[9] *Geiger T.*: Metallographische Untersuchungen an den Überhitzerrohren des Kessels Reutlingen nach verschiedenen Betriebszeiten Vortragsveranstaltung der Mannesmann Röhrenwerke AG, Düsseldorf 1958 p. 77–80

[10] *Huber H.*: Abzunderungsschäden im Kessel Reutlingen Vortragsveranstaltung der Mannesmann Röhrenwerke AG, Düsseldorf 1958 p. 69–76

[11] *Baumann K.*: Korrosion und Korrosionsschutz auf der Rauchgasseite von Dampferzeugern VGB Kraftwerkstechnik Jahrgang 55 Heft 3 1975 p. 175–180

[12] *Meyer B., Willems O., Röper B.*: Mechanismen der chlorinduzierten Korrosion von Wirbelschicht-Heizflächen VGB Kraftwerkstechnik Jahrgang 75 Heft 12 1995 p. 1043–1048

[13] VGB 1999 — Verband der Großkraftwerksbetreiber: Maßnahmen zur Verminderung der Heizflächenabzehrung in abfallgefeuerten Dampferzeugern VGB Merkblatt M205 Essen 1999

[14] *Spiegel W., Herzog Th., Magel G., Müller W., Schmidl W.*: Dynamische chlorinduzierte Hochtemperaturkorrosion von Verdampfer- und Überhitzerbauteilen aufgrund spezieller Belagsentwicklung in VGB PowerTech Jahrgang 85 Heft 1/2 2005 p. 89–97

[15] *Hohmann U., Mohr G.*: Hochtemperaturkorrosion in Biomassekesseln in VGB PowerTech Jahrgang 85 Heft 6 2005 p. 47–52

[16] *Huenert D., Schulz W. Kranzmann A.*: Corrosion of Steels in H_2O–CO_2 atmosphere at temperatures between 500°C and 700°C. ICPWS XV Berlin, 08–11 Septermber 2008

[17] *Bordenet B., Kluger F.*: Thermodynamic Modelling of the Corrosive Deposits in Oxy-Fuel Fired Boilers. In Material Science Forum Vol. 595–598 / 2008 p. 261–269